

Reconfigurable Mott electronics for homogeneousneuromorphic platform

Zhen Yang(杨振), Ying-Ming Lu(路英明), and Yu-Chao Yang(杨玉超)
Citation: Chin. Phys. B, 2023, 32 (**12**): 128401. DOI: 10.1088/1674-1056/ad02e8
Journal homepage: http://cpb.iphy.ac.cn; http://iopscience.iop.org/cpb

What follows is a list of articles you may be interested in

Observation of size-dependent boundary effects in non-Hermitian electric circuits

Luhong Su(苏鹭红), Cui-Xian Guo(郭翠仙), Yongliang Wang(王永良), Li Li(李力), Xinhui Ruan(阮馨慧), Yanjing Du(杜燕京), Shu Chen(陈澍), and Dongning Zheng(郑东宁)
Chin. Phys. B, 2023, 32 (**3**): 038401. DOI: 10.1088/1674-1056/aca9c4

Memristor's characteristics: From non-ideal to ideal

Fan Sun(孙帆), Jing Su(粟静), Jie Li(李杰), Shukai Duan(段书凯), and Xiaofang Hu(胡小方)
Chin. Phys. B, 2023, 32 (**2**): 028401. DOI: 10.1088/1674-1056/ac7548

Suppression of ferroresonance using passive memristor emulator

S Poornima
Chin. Phys. B, 2021, 30 (**6**): 068401. DOI: 10.1088/1674-1056/abd7e0

Optoelectronic memristor for neuromorphic computing

Wuhong Xue(薛武红), Wenjuan Ci(次文娟), Xiao-Hong Xu(许小红), Gang Liu(刘钢)
Chin. Phys. B, 2020, 29 (**4**): 048401. DOI: 10.1088/1674-1056/ab75da

An ultra-wideband pattern reconfigurable antenna based on graphene coating

YanNan Jiang(姜彦南), Rui Yuan(袁锐), Xi Gao(高喜), Jiao Wang(王娇), SiMin Li(李思敏), Yi-Yu Lin(林诒玉)
Chin. Phys. B, 2016, 25 (**11**): 118402. DOI: 10.1088/1674-1056/25/11/118402

SPECIAL TOPIC — Post-Moore era: Materials and device physics

Reconfigurable Mott electronics for homogeneous neuromorphic platform

Zhen Yang(杨振)[1], Ying-Ming Lu(路英明)[1], and Yu-Chao Yang(杨玉超)[1,2,3,4,†]

[1] *Beijing Advanced Innovation Center for Integrated Circuit, School of Integrated Circuits, Peking University, Beijing* 100871, *China*
[2] *School of Electronic and Computer Engineering, Peking University, Shenzhen* 518055, *China*
[3] *Center for Brain Inspired Chips, Institute for Artificial Intelligence, Frontiers Science Center for Nano-optoelectronics, Peking University, Beijing* 100871, *China*
[4] *Center for Brain Inspired Intelligence, Chinese Institute for Brain Research (CIBR), Beijing* 102206, *China*

(Received 5 August 2023; revised manuscript received 28 September 2023; accepted manuscript online 13 October 2023)

To simplify the fabrication process and increase the versatility of neuromorphic systems, the reconfiguration concept has attracted much attention. Here, we developed a novel electrochemical VO_2 (EC-VO_2) device, which can be reconfigured as synapses or LIF neurons. The ionic dynamic doping contributed to the resistance changes of VO_2, which enables the reversible modulation of device states. The analog resistance switching and tunable LIF functions were both measured based on the same device to demonstrate the capacity of reconfiguration. Based on the reconfigurable EC-VO_2, the simulated spiking neural network model exhibited excellent performances by using low-precision weights and tunable output neurons, whose final accuracy reached 91.92%.

Keywords: Mott electronics, reconfigurable, neuromorphic computing, VO_2

PACS: 84.30.–r, 85.40.–e, 87.85.dq, 81.07.–b **DOI:** 10.1088/1674-1056/ad02e8

1. Introduction

With the rapid developments of deep learning (DL),[1–3] the conventional hardware systems based on the CMOS circuits and von Neumann architecture suffered from severe delay and huge energy costs, especially when processing more huge volume of data.[4–7] To solve the problems, researchers start to learn from the human brain, which is better at processing complex cognitive issues with tiny energy costs.[8–10] These new computing paradigms are referred to as neuromorphic computing.[11,12] For instance, one important feature of computing in the brain is the integration of storage and processing, and lots of research has been devoted to constructing crossbar arrays based on emerging nonvolatile memories, which aim to accelerate multiplyaccumulate operations that dominated mostly in DL.[13–16]

The mostly studied artificial neural network (ANN) is a high level of abstraction of real neural networks in the human brain. To fully tap the potential of the brain, an SNN model was proposed, which has more similar structures to the brain than that of ANN.[17–20] Recently, there was some related hardware-accelertation of SNN or ANN.[21–27] The most obvious advantage of SNN is the ultra-low energy cost for the event-triggered characteristic. In the hardware implementation of SNN, the main components, synapses and neurons, are usually based on different materials and structures. The different-hardware based units will constrain the extension of network structures and functions.[28] Recently, there were some studies about reconfigurable neuromorphic devices for adaptive computing.[29–32] Through the same material system, the fabrication process of the neuromorphic systems can also be simplified. However, research on developing reconfigurable neuromorphic units for SNN is still scarce, and most of the existing approaches to reconfiguring still rely on extra electronic operations.[29,30]

Based on the above background and challenge, we designed a novel reconfigurable Mott device, which mainly consists of a VO_2 channel and LiPON electrolyte. The mechanism of channel resistance switching was clarified by material characterization and DFT calculations. Under the different operation modes, the EC-VO_2 device could be configured as synapses and tunable LIF neurons, the reconfiguration between different roles does not require any extra operations. At last, image classification was successfully implemented on the reconfigurable-EC-VO_2-based platform.

2. Experimental detail

The studied EC-VO_2 device was fabricated on the Al_2O_3 substrates. Firstly, 40 nm VO_2 films were epitaxially grown by pulsed-laser deposition (PLD) technique; after that, 5 nm Ti and 25 nm Au were deposited on VO_2 films through electron-beam evaporation, in which electron-beam lithography was used for patterning. Then, the second electron-beam lithography process was carried out to pattern the active region, 180 nm LiPON and 20 nm SiO_x were sequentially deposited

†Corresponding author. E-mail: yuchaoyang@pku.edu.cn

© 2023 Chinese Physical Society and IOP Publishing Ltd

by magnetron sputtering. After the lift-off process, 10 nm Ti and 220 nm Au were deposited using electron-beam evaporation to form testing pads. Finally, the three-terminal EC-VO_2 device was completed after the last lift-off process. All the electrical measurements were performed using an Agilent B1500A semiconductor parameter analyzer.

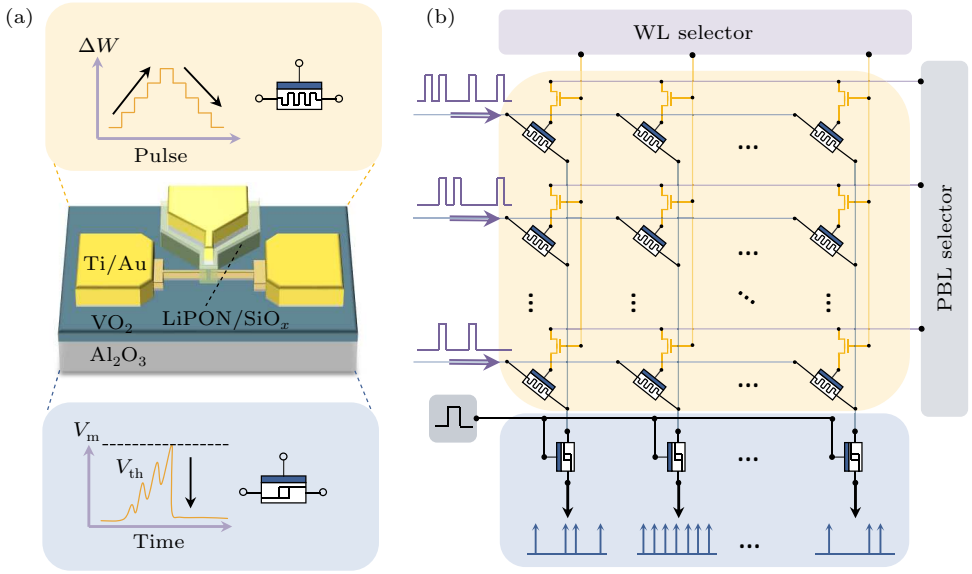


Fig. 1. The schematic of the homogeneous hardware platform based on reconfigurable Mott electronics. (a) Structure schematics of configuring as synapse or neuron units based on the same three-terminal EC-VO_2 device. (b) The designed hardware systems for SNN implementation with reconfigurable EC-VO_2 devices.

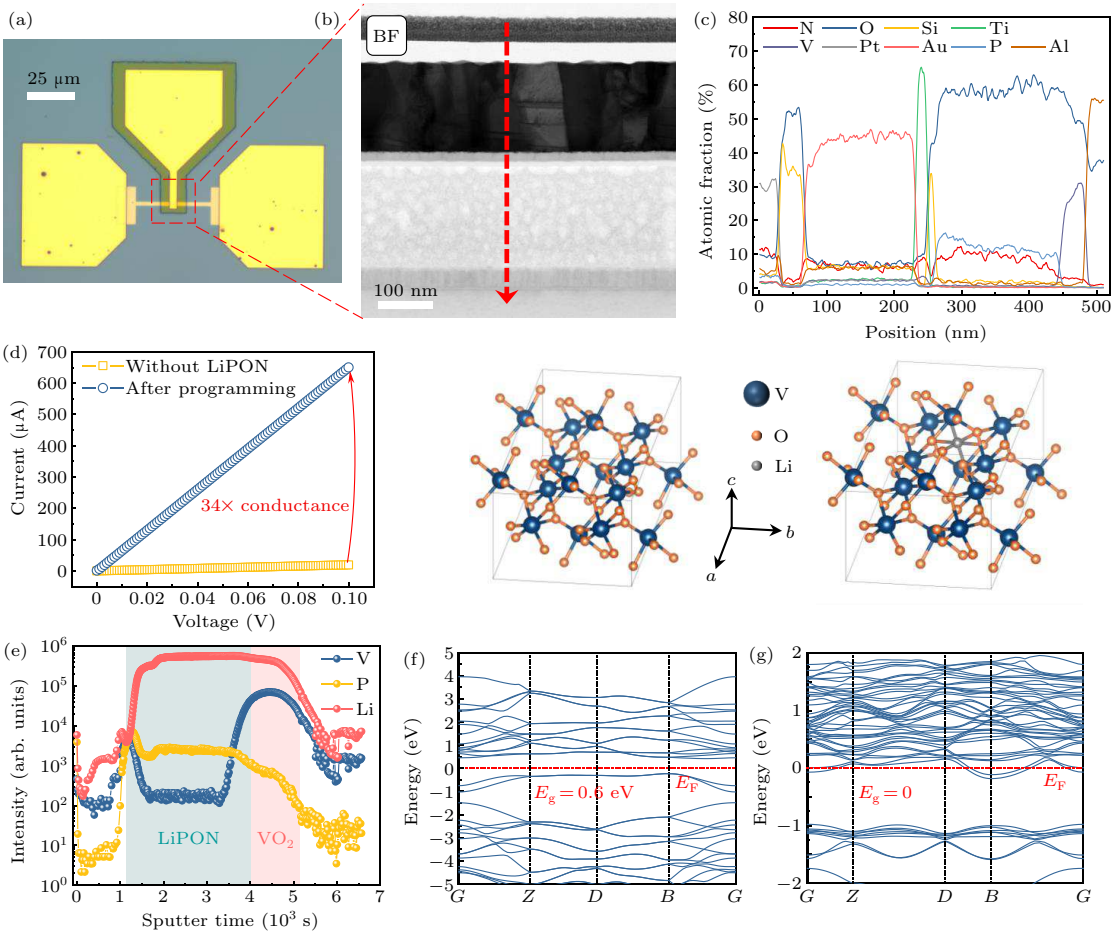


Fig. 2. Material characterization and DFT calculations of electrochemical doping. (a) Optical photograph of fabricated EC-VO_2 device. (b) The cross-sectional TEM image of the active region in the EC-VO_2 device, as indicated within the red box in panel (a). (c) Elemental mapping of different layers within the device through the red arrows in panel (b). (d) The initial conductance DC sweep of the EC-VO_2 channel before LiPON deposition and after programming under positive gate voltages. (e) TOF-SIMS results of the EC-VO_2 device after programming, in which the Li ions are intercalated into the VO_2 layer. DFT calculations of the energy band structure of (f) pure M1 phase VO_2 and (g) Li-doping VO_2, which verifies the increase of electrical conductivity after ionic doping.

3. Results and discussion

The fabricated EC-VO_2 devices are shown in Fig. 2(a), the gate pad is limited within the electrolyte region to avoid interferences with channel areas. The cross-sectional transmission electron microscope image of the device's active region is presented in Fig. 2(b), and the corresponding line scan of elemental mappings (Fig. 2(c)) verifies the material components. To form an amorphous LiPON fast ion conductor, we introduce nitrogen atoms into the initial lithium phosphate crystals, aiming to increase the reticular crosslinking structure.[32] To clarify the mechanisms of channel conductance modulation, material characterization with DFT calculation is employed to unveil that. As shown in Fig. 2(d), the conductance of the programmed device increases 34 times more than the device without electrolyte capped, both active regions of devices are kept at 60 μm × 60 μm. Time-of-flight secondary ion mass spectrometry (ToF-SIMS) characterization (Fig. 2(e)) of the programmed EC-VO_2 device demonstrates the intercalation of Li ions into the VO_2 lattice. Given the small volume of Li ions, the doping positions are most probably at the interstitial sites.[33] The two material models are constructed in Figs. 2(f) and 2(g). In Fig. 2(f), the energy band structure of pure M1 phase VO_2 indicates a 0.6 eV gap, however, after introducing Li ions, the vanish of the band gap illustrated the increase of the electrical conductivity (Fig. 2(g)). According to previous related research,[26] the introduction of Li ions can help weaken the binding strength between V ions and O ions, which can increase the concentration of free V_{3d} electrons and overall carriers in the material systems.

3.1. Multi-tunable states for configuring as synapses

By utilizing dynamic ionic doping, the reversible channel conductance modulation can be realized, which can be configured as synapses in neural networks to implement in-memory computing. Figure 3(a) shows the typical testing schematics, the modulation signal in the gate terminal can control the doping or dedoping of Li ions in the VO_2 channel. As demonstrated in Figs. 3(b) and 3(c), under the positive (or negative) gate voltage sweep, the channel conductance will get increased (or decreased) with Li ions moved into (or extracted from) the channel. The long-term potentiation and depression under continuous gate pulses are performed in Fig. 3(d), the multi states can be employed to accelerate the matrix-vector product through Ohm's law and Kirchhoff's law. The retention tests in Fig. 3(e) indicate the nonvolatile state changes under ionic doping, which can help hardware systems store the neural network weights even after the blackout. To realize full-analog computing, the linearity of different states under small reading bias is also tested in Fig. 3(f), further proving the feasibility of EC-VO_2 configured as synaptic devices.

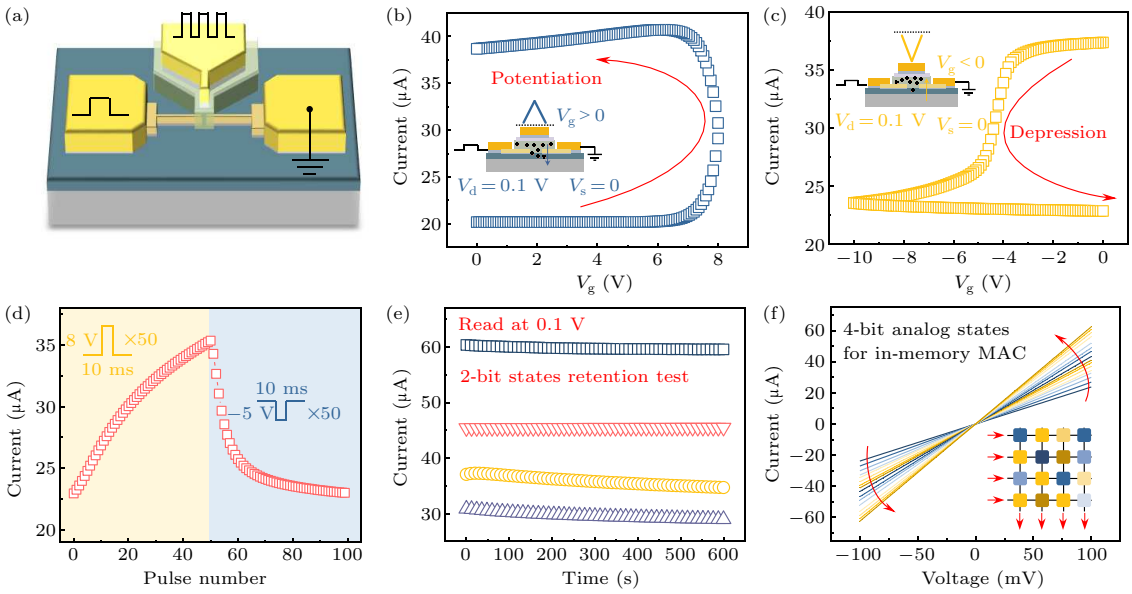


Fig. 3. Electrical characteristics of EC-VO_2 devices configured as synapses. (a) Typical testing schematics of synaptic properties, in which modulating signal is applied on the gate terminal and monitoring bias is applied on the drain terminal with source terminal grounded. The transfer curves of a (b) positive V_g sweep or (c) negative V_g sweep, with 0.1 V bias monitoring the channel conductance changes. (d) Long-term potentiation and depression under 50 pulses of 8 V and −5 V, whose widths are both set as 10 ms and monitoring read voltage is set at 0.1 V. (e) The retention performances of four distinguished states with a recording time of 600 s. (f) Linear-reading tests of 4-bit states for analog in-memory computation.

3.2. Tunable threshold-switching (TS) properties for configuring as neurons

There was plenty of research about utilizing VO_2 as LIF neurons,[34–36] so we can also change the role of EC-VO_2 from synapses to neurons. As shown in Fig. 4(a), when testing EC-VO_2 as neurons, the gate terminal and source terminal are both grounded, and the signals or connections with load resistors are placed at the drain terminal. Different from most of the previous two-terminal VO_2 devices, the third terminal can be used to modulate the channel resistances and further

tune the TS behaviors. As demonstrated in Figs. 4(b) and 4(c), the threshold voltage (V_{th}) will get reduced along with the lowering of initial channel resistances, while the hold voltage (V_{hold}) keeps still regardless of the initial states. Based on the previous research explaining the threshold-switching mechanisms, the insulator–metal transition (IMT) after the internal temperature reaches a critical point dominates. Ionic doping can only change the high-resistance states (HRS) before IMT while the low-resistance states (LRS) all keep almost the same at the conductive rutile phase. As the HRS decreases, to keep the heating power at the same level, the applied voltage will also be lower, which corresponds to the decrease of V_{th}; under the same LRS, the V_{hold} will keep almost unchanged when the heating power is below a certain level. The tunable V_{th} provides a more degree of freedom in designing the LIF neurons in neural networks.

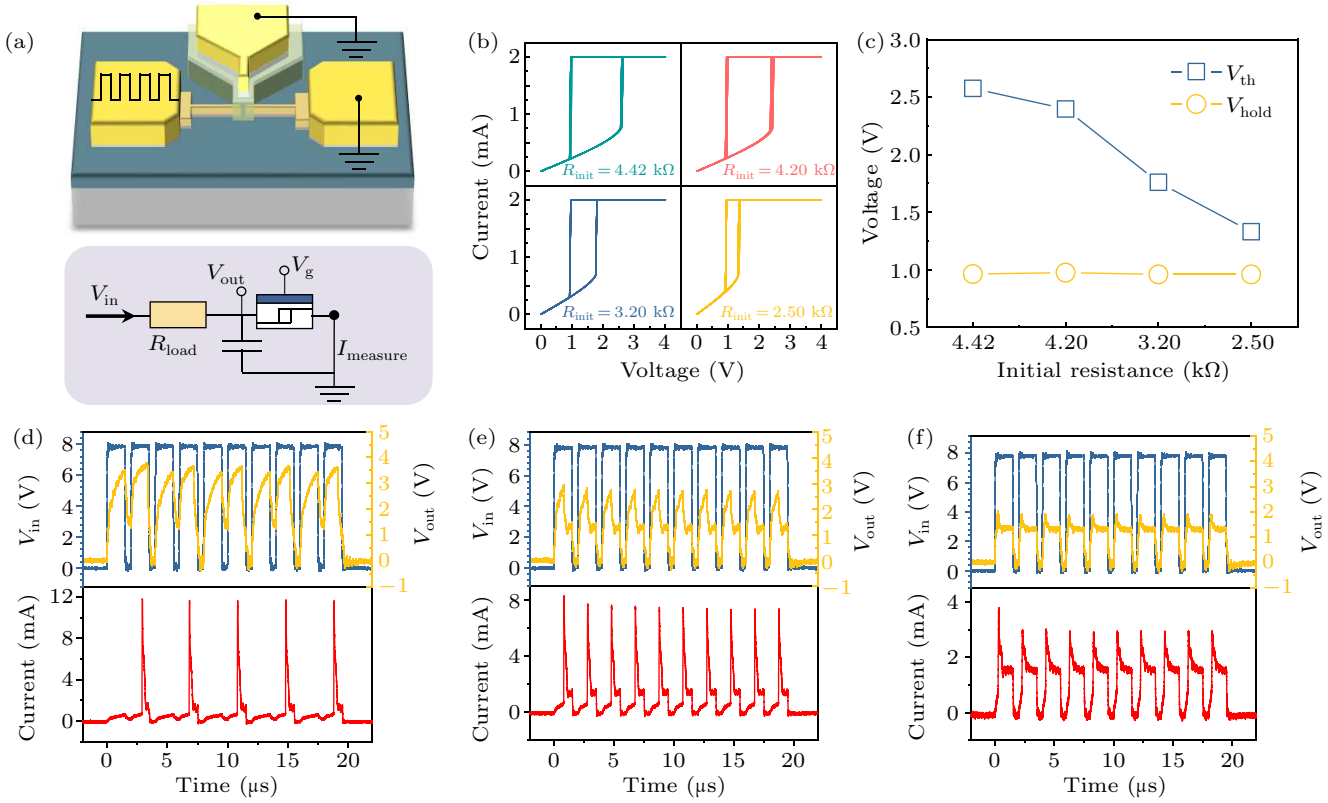


Fig. 4. Electrical characteristics of EC-VO_2 devices configured as neurons. (a) Typical measurement schematics of testing neuronic properties, for which multi stimuli are applied at drain terminal with gate and source grounded. (b) Different *I*–*V* curves for different initial channel resistances, each state was tested 25 cycles and exhibited stable TS behaviors. (c) Average V_{th} and V_{hold} in panel (b) for corresponding initial resistance, which shows different relationships. The LIF neuron functions of different V_{th} at (d) 3.6 V, (e) 2.8 V and (f) 1.9 V, with load resistance fixed at 4 kΩ.

The LIF neuron function tests of different V_{th} at 3.6 V, 2.8 V and 1.9 V are shown in Figs. 4(d), 4(e) and 4(f), respectively. The following equation can describe the LIF neuron circuits:

$$C_m \frac{dV_{out}}{dt} = \frac{V_{in} - V_{out}}{R_L} - \frac{V_{out}}{R_{VO_2}},$$

where C_m is the capacitance in parallel to the VO_2 device or can be parasitic capacitance, V_{out} is the output voltage in Fig. 4(a) or membrane voltage, V_{in} is the input voltage in Fig. 4(a). R_{VO_2} represents the channel resistance of EC-VO_2 and R_L denotes the load resistance of the LIF neuron circuits. When the V_{out} reaches beyond V_{th}, the R_{VO_2} will change from HRS to LRS sharply, along with a sudden increase of current flowing from VO_2, which is also termed as firing. From Figs. 4(d)–4(f), the different firing frequencies and leaky-integrate behaviors result from different V_{th} and initial HRS, which can be adaptive to different realistic environments.

3.3. Large-scale SNN based on the reconfigurable Mott electronics

Based on the above discussions, we construct an SNN model based on the reconfigurable Mott electronics (Figs. 1(b) and 5(a)), whose structure is set as a 748–10 fully connected network. The Poisson encoder is employed to encode the image intensities of Modified National Institute of Standards and Technology (MNIST) datasets to a set of spike trains, which follow the Poisson distribution. The subthreshold dynamics of output LIF neurons are defined as

$$\tau \frac{dV_m}{dt} = -(V_m - V_{rest}) + I(t),$$

where V_m denotes the membrane voltage of the LIF neurons, V_{rest} represents the resting potential, τ is the membrane time

constant, and $I(t)$ is the input to neurons at time t. When the membrane voltage V_m exceeds the threshold voltage V_{th}, the neuron will elicit a spike. Compared with the dynamic equation of the LIF neuron circuits based on VO_2, the similarity enables direct hardware realization. To update the connected weights, the backpropagation through time (BPTT) and surrogate function are used to calculate the gradients.

When using the ECVO$_2$ as weights, the realistic state number needs to be considered (Figs. 3(d) and 3(f)), so we adopt the symmetrically uniform quantized methods and differential cell structure, the Gaussian noises of 0.01 standard variation are also added into the quantized weights while keeping the V_{th} at 1.0, the final testing accuracies of different weight precision are presented in Fig. 5(b). When the weight precision exceeds 2 bits, the performances will reach saturation, and the state of EC-VO$_2$ can realize more than 16 distinguished states (4 bits), so it can easily meet the requirement of quantized weight precision. In Fig. 5(c), the final testing accuracy of 3-bit precision can reach 91.92%, and the quantized weights also have an apparent boundary. In conventional two-terminal TS devices, the threshold voltage is usually fixed after fabrication, so it is hard to change the V_{th} to realize device-algorithm co-optimization in different situations. Based on our electrochemical modulation of the VO_2 parameters, the V_{th} can be tuned continuously by lowering the initial states (Fig. 5(d)). The network performances of different threshold voltages and fixed 3-bit weight precision are demonstrated in Fig. 5(e), which indicates the accuracies can be enhanced by setting the proper threshold voltage. Specifically, the threshold voltage value is different from the V_{th} of EC-VO$_2$, in which a linear scaling factor relates them, so in the realistic mapping of model parameters into hardware platforms, the scaling factor is worth carefully considering.

Finally, after finishing training the SNN in Fig. 5(c), the number 5 is used to test the performances. As shown in Figs. 5(f) and 5(g), the frequency of spike firing in neuron 5 is the maximum among all the output neurons, which proved the model realizes the successful classification.

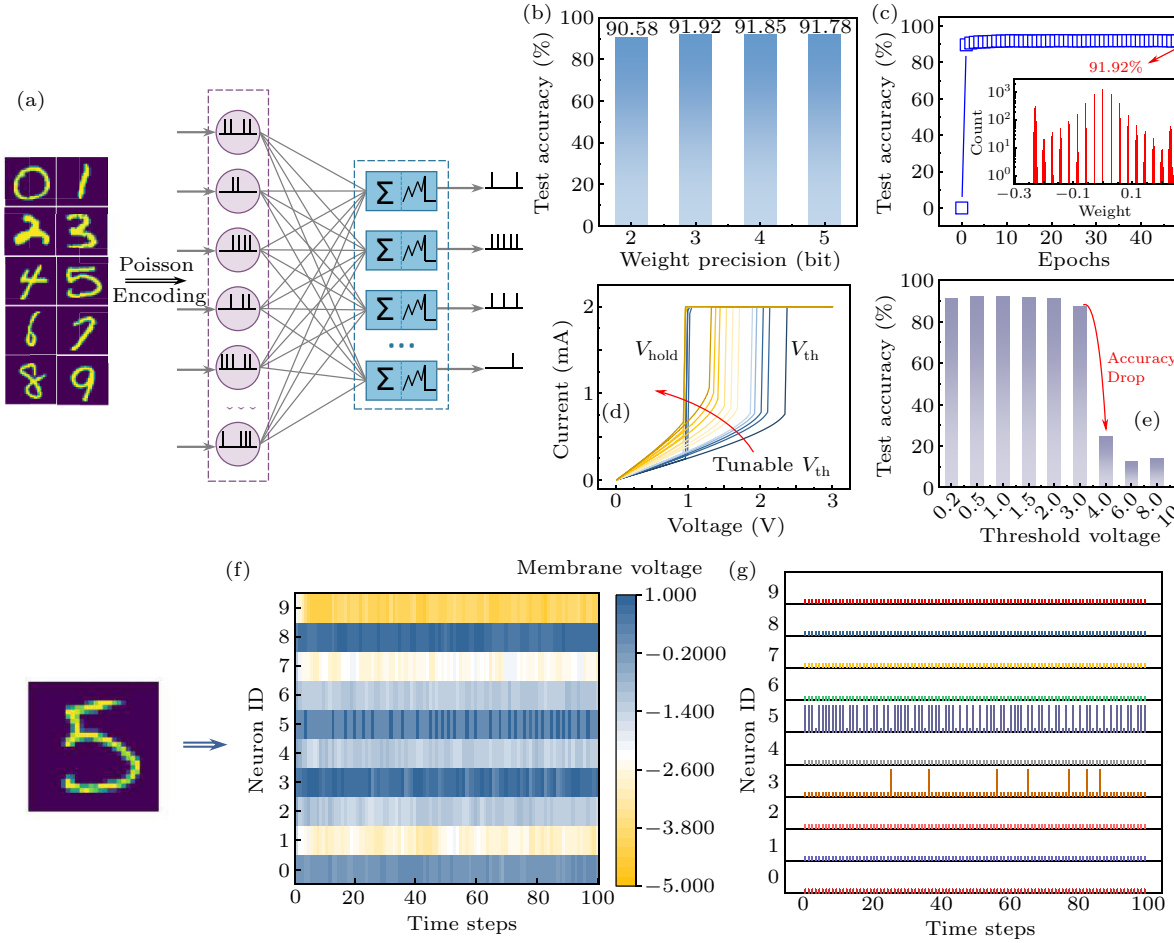


Fig. 5. The network-level performances based on the reconfigurable Mott electronics. (a) The network structure of the designed SNN, in which the Poisson encoder was employed to encode the MNIST images into a sequence of pulses. (b) The final test accuracies of different weight precision from 2 bits to 5 bits, with threshold voltage fixed at 1.0. (c) The evolution of test accuracy with training epochs, where the weight precision was chosen at 3 bits and threshold voltage was set at 1.0, the inset shows the final weight distribution after finishing the network training. (d) The measured multi I–V curves of different V_{th}, show the capacity of continuously modulating threshold voltages, which provide a more tunable parameter in enhancing the neural network performances. (e) The final testing accuracies of different defined threshold voltage in output neurons. (f) Testing results of classifying the number 5 after training in panel (c), both the evolution of (f) membrane voltages and (g) firing spikes with time steps can verify the successful classification.

4. Conclusion and perspectives

We propose and fabricate a kind of novel reconfigurable Mott electronics for constructing a homogeneous neuromorphic platform. By utilizing electrochemical ionic doping, the resistance of VO_2 can be reversibly modulated. On one hand, the nonvolatile resistance switching can be used as synapses to accelerate matrix-vector multiplication; on the other hand, the TS switching with electrochemical modulation can be configured as tunable LIF neurons. Based on the versatile EC-VO_2, a low-precision SNN model is developed, and combined with a properly designed threshold voltage, we successfully achieve high accuracy of image classification. Our work paves a new way for designing a homogeneous neuromorphic hardware platform to reduce process costs and enhance the flexibility of reconfiguration.

Acknowledgments

Project supported by the National Natural Science Foundation of China (Grant Nos. 61925401, 92064004, 61927901, and 92164302) and the 111 Project (Grant No. B18001). Y. Y. acknowledges support from the Fok Ying-Tong Education Foundation and the Tencent Foundation through the XPLORER PRIZE. The authors acknowledge the support of TOF-SIMS characterization by Dr. Tinglu Song and the first-principal computation by Dr. Bing Zheng from Beijing Institute of Technology.

References

[1] LeCun Y, Bengio Y and Hinton G 2015 *Nature* **521** 436
[2] Mankowitz D J, Michi A, Zhernov A, *et al.* 2023 *Nature* **618** 257
[3] Yu S 2018 *Proc. IEEE* **106** 260
[4] Merolla P A, Arthur J V, Alvarez-Icaza R, Cassidy A S, Sawada J, Akopyan F, Jackson B L, Imam N, Guo C, Nakamura Y, Brezzo B, Vo I, Esser S K, Appuswamy R, Taba B, Amir A, Flickner M D, Risk W P, Manohar R and Modha D S 2014 *Science* **345** 668
[5] Zidan M A, Strachan J P and Lu W D 2018 *Nat. Electron.* **1** 22
[6] Huang X H, Liu C S, Jiang Y G and Zhou P 2020 *Chin. Phys. B* **29** 078504
[7] Sebastian A, Gallo M L, Aljameh R K and Eleftheriou E 2020 *Nat. Nanotechnol.* **15** 529
[8] Yao P, Wu H Q, Gao B, Tang J S, Zhang Q T, Zhang W Q, Yang J J and Qian H 2020 *Nature* **577** 641
[9] Duan Q X, Jing Z K, Zou X L, Wang Y H, Yang K, Zhang T, Wu S, Huang R and Yang Y C 2020 *Nat. Commun.* **11** 3399
[10] Liu K Q, Zhang T, Dang B J, Bao L, Xu L Y, Cheng C D, Yang Z, Huang R and Yang Y C 2022 *Nat. Electron.* **5** 761
[11] Marković D, Mizrahi A, Querlioz D and Grollier J 2020 *Nat. Rev. Phys.* **2** 499
[12] Liu R, He Y L, Jiang S S, Zhu L, Chen C S, Zhu Y and Wan Q 2021 *Chin. Phys. B* **30** 058102
[13] Wang X, Ge C, Li G, Guo E J, He M, Wang C, Yang G Z and Jin K J 2020 *Chin. Phys. B* **29** 098101
[14] Strukov D B, Snider G S, Stewart D R and Williams R S 2008 *Nature* **453** 80
[15] Wang Z R, Wu H Q, Burr G W, Hwang C S, Wang K L, Xia Q F and Yang J J 2020 *Nat. Rev. Mater.* **5** 173
[16] Kumar S, Wang X X, Strachan J P, Yang Y C and Lu W D 2022 *Nat. Rev. Mater.* **7** 575
[17] Zhang X M, Zhuo Y, Luo Q, Wu Z H, Midya R, Wang Z R, Song W H, Wang R, Upadhyay N K, Fang Y L, Kiani F, Rao M Y, Yang Y, Xia Q F, Liu Q, Liu M and Yang J J 2020 *Nat. Commun.* **11** 51
[18] Prezioso M, Mahmoodi M R, Bayat F M, Nili H, Kim H, Vincent A and Strukov D B 2018 *Nat. Commun.* **9** 5311
[19] Zhang X M, Wang W, Liu Q, Zhao X L, Wei J S, Cao R R, Yao Z H, Zhu X L, Zhang F, Lv H B, Long S B and Liu M 2018 *IEEE Electron Dev. Lett.* **39** 308
[20] Dev D, Krishnaprasad A, Shawkat M S, He Z Z, Das S, Fan D L, Chung H S, Jung Y and Roy T 2020 *IEEE Electron Dev. Lett.* **41** 936
[21] Xu X X, Luo Q, Gong T C, Lv H B, Liu Q and Liu M 2021 *Chin. Phys. B* **30** 058702
[22] Li W H, Lan X K, Liu X H, Zhang E Z, Deng Y C and Wang K Y 2022 *Chin. Phys. B* **31** 117106
[23] Lin X H, Long H T, Ke S, Wang Y Y, Zhu Y, Chen C S, Wan C J and Wan Q 2022 *Chin. Phys. Lett.* **39** 068501
[24] Zhao Y H, Liu B, Yang J L, He J and Jiang J 2020 *Chin. Phys. Lett.* **37** 088501
[25] Zhou H J, Li Y and Miao X S 2022 *Sci. China Inf. Sci.* **65** 122410
[26] Cheng C D, Tiw P J, Cai Y M, Yan X Q, Yang Y C and Huang R 2021 *Sci. China Inf. Sci.* **64** 221402
[27] Zhu Y, He Y L, Chen C S, Zhu L, Wan C J and Wan Q 2022 *Sci. China Inf. Sci.* **65** 162401
[28] Wang Z R, Joshi S, Yang J J, *et al.* 2018 *Nat. Electron.* **1** 137
[29] Zhang H T, Park T J, Ramanathan S, *et al.* 2022 *Science* **375** 533
[30] Fu Y Y, Zhou Y, Huang X D, Dong B Y, Zhuge F W, Li Y, He Y L, Chai Y and Miao X S 2022 *Adv. Funct. Mater.* **32** 2111996
[31] Wang T Y, Meng J L, Zhou X F, Liu Y, He Z Y, Han Q, Li Q X, Yu J J, Li Z H, Liu Y K, Zhu H, Sun Q Q, Zhang D W, Chen P N, Peng H S and Chen L 2022 *Nat. Commun.* **13** 7432
[32] Yang Z, Zhang T, Liu K Q, Dang B J, Xu L Y, Yang Y C and Huang R 2023 *Adv. Intell. Syst.* **5** 2300026
[33] Chen Y L, Wang Z W, Chen S, Ren H, Li B W, Yan W S, Zhang G B, Jiang J and Zou C W 2018 *Nano Energy* **51** 300
[34] Yuan R, Duan Q X, Tiw P J, Li G, Xiao Z J, Jing Z K, Yang K, Liu C, Ge C, Huang R and Yang Y C 2022 *Nat. Commun.* **13** 3973
[35] Yuan R, Tiw P J, Cai L, Yang Z Y, Liu C, Zhang T, Ge C, Huang R and Yang Y C 2023 *Nat. Commun.* **14** 3695
[36] Deng S B, Yu H M, Park T J, Islam A N, Manna S, Pofelski A, Wang Q, Zhu Y M, Sankaranarayanan S, Sengupta A and Ramanathan S 2023 *Sci. Adv.* **9** 4838